Electronic structure and magnetism in half-Heusler compounds

2003 J. Phys.: Condens. Matter 15 7307

(http://iopscience.iop.org/0953-8984/15/43/014)

INSTITUTE OF PHYSICS PUBLISHING JOURNAL OF PHYSICS: CONDENSED MATTER

J. Phys.: Condens. Matter **15** (2003) 7307–7323 PII: S0953-8984(03)63660-X

Electronic structure and magnetism in half-Heusler compounds

B R K Nanda and I Dasgupta[1]

Department of Physics, Indian Institute of Technology Bombay, Powai, Mumbai 400 076, India

E-mail: dasgupta@phy.iitb.ac.in

Received 19 May 2003
Published 17 October 2003
Online at stacks.iop.org/JPhysCM/15/7307

Abstract

In this paper we have applied the full-potential linearized muffin tin orbital method and the tight-binding linearized muffin tin orbital method to investigate in detail the electronic structure and magnetism of a series of half-Heusler compounds XMZ with X = Fe, Co, Ni, M = Ti, V, Nb, Zr, Cr, Mo, Mn and Z = Sb, Sn. Our detailed analysis of the electronic structure using various indicators of chemical bonding suggests that covalent hybridization of the higher-valent transition element X with the lower-valent transition element M is the key interaction responsible for the formation of the d–d gap in these systems. However, the presence of the sp-valent element is crucial to provide stability to these systems. The influence of the relative ordering of the atoms in the unit cell on the d–d gap is also investigated. We have also studied in detail some of these systems with more than 18 valence electrons which exhibit novel magnetic properties, namely half-metallic ferro- and ferrimagnetism. We show that the d–d gap in the paramagnetic state, the relatively large X–Sb hybridization and the large exchange splitting of the M atoms are responsible for the half-metallic property of some of these systems.

1. Introduction

Multinary materials with complex crystal structures exhibiting unusual electronic and magnetic properties have always attracted considerable experimental and theoretical attention with a view to harnessing these unconventional properties into possible device applications. One such group of materials which is being actively investigated at the moment are the half-Heusler compounds. The parent Heusler compounds with the general formula X_2YZ, where X and Y are transition metals and Z is an sp-valent element, have received considerable attention in the past due to their interesting and diverse magnetic properties [1]. The half-Heusler phases have the same cubic structure, except that one of the sites occupied by the X atom in the parent

[1] Author to whom any correspondence should be addressed.

compound is empty, giving a general formula XYZ. The absence of inversion symmetry due to an empty X site and the low coordination number of the d-band metals in the half-Heusler alloys are believed to be important for the novel electronic and magnetic properties of these materials. One such property, half-metallic ferromagnetism, was discovered by de Groot *et al* [2] in the Mn-based half-Heusler alloy NiMnSb. In a half-metallic ferromagnet the minority band is semiconducting with a gap at the Fermi level, implying complete spin polarization at the Fermi surface. Recently the rapid development of magnetoelectronics [3] has intensified the interest in such compounds, as they are promising candidates for engineering new spintronics devices such as quantum sensors, quantum resistors and quantum computers in the near future. In addition, the discovery of good thermoelectric properties [4–8] in the Ni-, Co- and Fe-based half-Heusler compounds has initiated a lot of study in these systems. The narrow band gap at the Fermi level in some of these compounds with 18 valence electrons and voids in the crystal structure are believed to be the key ingredients making these materials promising candidates for thermoelectric applications. In this context first-principles electronic structure calculations are proving to be a useful tool in sorting out the mechanism, that lead to useful properties in complex materials.

The family of half-Heusler compounds of the form XMZ with X = Fe, Co, Ni, M = Ti, V, Cr, Mn, Zr, Nb, Mo and Z a pnictide or stannide ion (Sb, Sn) are intriguing because despite all the elements being metallic some of them, depending on the number of valence electrons, are either semiconducting or half-metallic. The physical origin of the gap in the paramagnetic and spin-polarized state in these compounds is a crucial and subtle issue and is important for many of their interesting properties. Several electronic structure calculations [9–16], ranging from semiempirical extended Hückel type calculations to highly accurate full-potential screened KKR calculations, have been devoted to understanding the above issue. Further, it is also crucial to understand which factors (structural as well as chemical) influence the gap in these compounds as that will help to design materials with novel properties. From the structural point of view it has been found [9, 10, 14] that the relative ordering of the atoms in the unit cell plays a crucial role in the electronic structure of these systems, in particular it influences the gap. Calculations for the Ni-based compounds (NiMP), where M is a trivalent (Sc) or tetravalent (Ti, Zr, HF) ion and P is a pnictide or stannide ion (Sb, Sn), by Ogut and Rabe [9] and Larson *et al* [10] predict that the minimum energy configuration for these alloys occurs when the higher-valent element Ni occupies the octahedrally coordinated pocket of the NaCl substructure formed by the other two elements (MP). This relative arrangement of the atoms in the unit cell has been accepted in general for all the half-Heusler compounds. It remains to be understood why the relative position of the atoms in the unit cell has such a profound influence on the gap. The lattice parameter and the reduced dimensionality (surfaces) are among the other issues which have been seen to influence the gap. The role of chemical substitution on the half-metallic character of these compounds has been recently investigated [16] and the conclusion has been that the substitution of the transition metal (TM) atoms may preserve the half-metallic character while substituting the sp atom results in a rigid shift of the bands with the Fermi level no longer at the gap in the minority spin channel. Hence a proper coordination of all these factors is crucial for engineering these materials for possible applications.

In this paper we have investigated in detail the electronic structure, chemical bonding and magnetism of a series of half-Heusler compounds, XMZ (X = Fe, Co, Ni, M = Ti, V, Nb, Zr, Cr, Mo, Mn, Z = Sn, Sb) in the light of the issues mentioned above. We have calculated the equilibrium lattice constants and determined the most stable crystallographic order for some of these compounds. Our total energy calculations are based on the highly accurate full-potential linearized muffin tin orbital method (FP-LMTO) developed by Savrasov [17] and the analysis of the electronic structure and chemical bonding is carried out in the framework

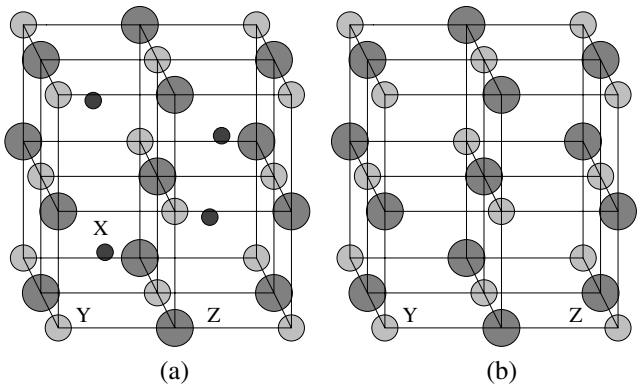

Figure 1. (a) Cubic half-Heusler structure. (b) Rock salt arrangement of YZ.

Table 1. Form of the binary substructures in α, β, γ phases.

Structure (phase)	X–M substructure	M–Z substructure	X–Z substructure
α	Diamond	NaCl	Diamond
β	NaCl	Diamond	Diamond
γ	Diamond	Diamond	NaCl

of the tight-binding linearized muffin tin orbital (TB-LMTO) method in the atomic sphere approximation (ASA) [18]. The rest of the paper is organized as follows. In section 2 we describe the crystal structure and the computational details for the FP-LMTO as well as TB-LMTO ASA calculations. A detailed analysis of the paramagnetic electronic structure is carried out in section 3. Section 4 contains a description of the spin-polarized electronic structure calculations and their analysis. Finally in section 5 we present our conclusions.

2. Structure and computational details

The half-Heusler compounds XYZ crystallize in the face-centred cubic structure with one formula unit per primitive cell, as shown in figure 1(a). The space group is $F4/3m$ (No 216). Fe, Co and Ni represent the X while M (Ti, V, Nb, Zr, Cr, Mo, Mn) and Sb/Sn represent the Y and Z respectively. In the conventional stable structure Y and Z atoms are located at $4a(0, 0, 0)$ and $4b(\frac{1}{2}, \frac{1}{2}, \frac{1}{2})$ positions forming the rock salt structure arrangement (see figure 1(b)) and the X atom is located in the octahedrally coordinated pocket, at one of the cube centre positions $4c(\frac{1}{4}, \frac{1}{4}, \frac{1}{4})$ leaving the other $4d(\frac{3}{4}, \frac{3}{4}, \frac{3}{4})$ empty. This creates voids in the crystal structure as mentioned earlier. The nearest neighbour coordination of the X atom is four M atoms and four Z atoms at a distance $\sqrt{3}a/4$. In addition, to this structure we have also investigated the stability for the configurations (i) ZMX with Sb/Sn occupying the octahedrally coordinated pocket and (ii) MXZ with the lower-valent transition element M occupying the octahedrally coordinated pocket. In analogy with Ogut and Rabe [9] and Larson *et al* [10] we shall designate the three configurations XMZ, ZMX and MXZ as α, β and γ respectively. In table 1 we list the various binary substructures for the different configurations.

As mentioned earlier, we have employed the highly accurate FP-LMTO method in the framework of GGA [19] to calculate the equilibrium lattice constants and energetics associated with the relative ordering of the atoms in the unit cell for some half-Heusler compounds.

The analysis of the electronic structure is carried out in the framework of the TB-LMTO-ASA. Below we provide some details of the FP-LMTO as well as TB-LMTO-ASA calculations.

For the FP-LMTO calculations, we have used a 3κ-spd LMTO basis set for each compound with one-centre expansions inside the MT sphere performed up to $l_{\max} = 6$. In the interstitial region the basis functions are expanded in plane waves. The induced charge densities and screened potentials are represented inside the MT sphere by spherical harmonics up to $l_{\max} = 6$ and in the interstitial region by plane waves (5064 plane waves) with the energy cut-off corresponding to a (26, 26, 26) fast Fourier transform grid in the unit cell of direct space. The Brillouin zone integration over the (16 16 16) k-mesh is performed by the tetrahedron method [20].

Self-consistent TB-LMTO-ASA calculations are done in the framework of LDA [21] as well as GGA [19]. The space filling in the ASA is achieved by inserting empty spheres in the cube centre positions ($\frac{3}{4}$, $\frac{3}{4}$, $\frac{3}{4}$) and by inflating the atom-centred non-overlapping spheres. The atomic radii are chosen in such a way that (i) the charge on the empty spheres is negligible and (ii) the overlap of the interstitial with the interstitial, atomic with the atomic and interstitial with the atomic spheres remains within the permissible limit of the ASA. The basis set for the self-consistent electronic structure calculation includes X, M(s, p, d), and Sb, Sn(s, p), the rest being downfolded. The (16, 16, 16) k-mesh has been used for self-consistency, and corresponds to 245 irreducible k-points. All the k-space integrations were performed using the tetrahedron method. In order to obtain a detailed understanding of the origin of various features in the electronic structure we have calculated the total and partial densities of states. While the partial densities of states provide us with information concerning the relative contributions of various orbitals at different energy regions, they cannot provide any k-dependent information. In order to obtain such momentum-related information we have additionally analysed the band dispersions and the orbital projected band structures, the so-called fat bands [22]. This analysis is supplemented to provide information regarding the specific pairs of atoms that participate in the bonding and the range of such interactions. This issue is addressed by computing the crystal orbital Hamiltonian population (COHP) [23] for various pairs of atoms, as it provides the relative contributions to bonding arising from different interactions in the system and therefore provides an energy-resolved visualization of chemical bonding.

3. Results and discussion

3.1. Structural properties

All the electronic structure calculations presented in this paper have been done using the experimental lattice constants. However, for some Fe- and Co-based compounds, namely FeCrSb, FeMnSb, FeMoSb and CoMoSb, where the experimental lattice constants are not available we have estimated theoretically the equilibrium lattice constants by performing the total energy minimization with the aid of the FP-LMTO method within GGA. The energy minimization is done for the most probable α configuration. Our results are displayed in table 2. Our estimate of the equilibrium lattice constants for the purpose of comparison for FeTiSn, FeTiSb and FeVSb are in excellent agreement with the available experimental lattice constants [1, 24, 25] and the deviation is found to be less than 1%. This suggests that for the compounds where the experimental lattice constant is not available our theoretical estimates will be very close to the experimental lattice constants if these compounds are synthesized in half-Heusler phases. Table 2 summarizes the number of valence electrons, the experimental and/or the theoretical lattice constants and some physical properties for all the compounds studied in this paper.

Table 2. Equilibrium lattice constants and band gaps for semiconductors (SC) as obtained from FP-LMTO calculations (VEC, valence electron count).

Compounds	VEC	Expt. lattice constant (au)	Equ. lattice constant (au)	Physical nature (theory)	Physical nature (expt)
FeTiSn	16	11.448	11.343	Metal	Metal
FeTiSb	17	11.260	11.237	Metal	Metal
FeVSb	18	11.013	10.985	SC (0.36 eV)	SC
FeCrSb	19	—	10.901	Half-metal	—
FeMoSb	19	—	11.183	Metal	—
FeMnSb	20	—	10.849	Half-metal	—
CoTiSb	18	11.122		SC (0.82 eV)	SC
CoZrSb	18	11.505		SC (0.83 eV)	SC
CoVSb	19	10.964		Metal	Metal
CoNbSb	19	11.146		Metal	Metal
CoMoSb	20	—	11.216	Metal	—
CoMnSb	21	11.105		Half-metal	Metal
NiTiSn	18	11.187		SC (0.136 eV)	SC
NiZrSn	18	11.546		SC (0.163 eV)	SC
NiTiSb	19	11.100		Metal	Metal
NiVSb	20	10.935		Metal	Metal
NiMnSb	22	11.200		Half-metal	Half-metal

Another important issue regarding the structural properties of the half-Heusler compounds that has attracted considerable attention is the relative arrangements of the atoms in the unit cell because the position of the atoms has a profound influence on the electronic structure. We have performed FP-LMTO GGA total energy calculations for three different configurations α, β and γ for the 18 valence electron count (VEC) compounds FeVSb, CoTiSb and NiTiSn with the available experimental lattice constant, and for the 20-VEC compound FeMnSb with the theoretically estimated lattice constant for the α phase. The results of our calculations are summarized in table 3, which unambiguously suggests that when the higher-valent transition element Fe/Co/Ni occupies the octahedrally coordinated site, i.e. the α configuration, the total energy is lowest. In this configuration the 18-electron compounds FeVSb, CoTiSb and NiTiSn display a gap at the Fermi level while the 20-electron compound FeMnSb is half-metallic. A similar finding has been reported by Ogut and Rabe [9] as well as by Larson *et al* [10] for the Ni-based compounds. We also note that for the Fe and the Co compounds the β phase is least stable. The energy difference between the β and the γ phase decreases as the higher-valent transition element changes from Fe to Ni and becomes negative for most Ni-based compound, as reported by Larson *et al* [10]. The gap close to the Fermi level exists only for the α configuration. The stability of the various configurations for the Ni-based compounds has been addressed by Larson *et al* [10] by considering the energetics of various binary subsystems. In this paper we shall consider the stability of various configurations by analysing the chemical bonding in these systems, to be described in the next section.

3.2. Paramagnetic electronic structure of XMSb

In this section we shall present the results of the TB-LMTO ASA electronic structure calculations for a series of Fe-, Co- and Ni-based half-Heusler compounds, XMSb, in the paramagnetic phase, for the most stable α configuration. In figure 2 we have displayed the total density of states for the compounds FeTiSb, FeVSb, FeMnSb, CoTiSb, CoVSb, CoMnSb, NiTiSb, NiVSb and NiMnSb with VEC ranging from 17 to 22 electrons. From figure 2 we

Table 3. Total energy difference in electronvolts for β and γ phases w.r.t. to the α phase.

Compound	Number of valence electrons	$E(\beta) - E(\alpha)$	$E(\gamma) - E(\alpha)$
FeVSb	18	2.99	1.85
CoTiSb	18	2.93	2.71
NiTiSn	18	2.48	2.49
FeMnSb	20	1.92	0.32

gather that the characteristic features of all half-Heusler compounds considered here are (i) a virtual gap far below the Fermi level and (ii) a gap at or very close to the Fermi level. It will be shown that the former is primarily due to the X(Fe, Co, Ni)-d–Sb-p interactions while the latter is a d–d gap resulting from the covalent hybridization of the higher-valent transition element X with the lower-valent transition element M. As we increase the number of valence electrons, the bands are progressively filled so that the 18-electron compounds are narrow gap semiconductors while the others with fewer or more than 18 valence electrons are metals in the paramagnetic phase. The states lying below the p–d gap are Sb p states. In fact, the Sb s state is lying further below the chosen scale of the figure. The states lying below and above the d–d gap are the bonding and antibonding states resulting from the covalent hybridization of X with M. The bonding bands are predominantly of X d character while the antibonding bands are predominantly M d character. Hence below the d–d gap there are nine bands (four Sb s + p, five predominantly X d) which in the paramagnetic state can accommodate 18 electrons. This is the reason that the gap lies at the edge of the Fermi level for the 18-electron compounds and makes them semiconducting. However, if there are more than 18 electrons the antibonding bands become occupied and the paramagnetic state may no longer be stable. Such instabilities may be alleviated by the formation of magnetic phases as we shall discuss later. The size of the p–d and the d–d gap varies for the Fe, Ni and Co compounds, and with the number of valence electrons. In the following section we shall analyse the chemical bonding of these compounds in detail to understand (i) the physical origin of the gap in these compounds and (ii) the reason for the α phase being the most stable structure.

3.3. The origin of the gap

In order to obtain insights into the origin of gap formation in these compounds we have considered the following binary substructure of the ternary compounds: X–Sb in the diamond structure and M–Sb in the NaCl structure. A similar strategy was also adopted by Ogut and Rabe [9] and Larson *et al* [10] to analyse the electronic structure of Ni-based half-Heusler compounds. We have chosen a representative compound, X = Fe and M = V, and our analysis remains the same for the other Fe-based compounds. Later in this section we shall compare our results with Co and Ni compounds.

We have displayed in figure 3 the band dispersion for the model binary compounds FeSb and VSb for the Bloch vector **k** along the high-symmetry points $\mathrm{L} = (2\pi/a)(0.5, 0.5, 0.5)$, $\Gamma(0, 0, 0)$, $\mathrm{X} = (2\pi/a)(0, 1, 0)$, $\mathrm{W} = (2\pi/a)(0.5, 1, 0)$ and $\mathrm{K} = (2\pi/a)(0, 0.75, 0.75)$. The bands are decorated with the specific orbital characters where the same band is plotted, but each band is given a width proportional to the (sum of the) weight(s) of the corresponding orthonormal orbital(s), which provides an access to the k-resolved visualization of the chemical bonding. We first consider the LDA band dispersion for the binary FeSb. We gather from figure 1(a) that in the absence of V the nearest neighbour coordination of Fe(Sb) is four Sb(Fe) which are at a distance of 4.77 au and the next nearest neighbour coordination for Fe(Sb) is

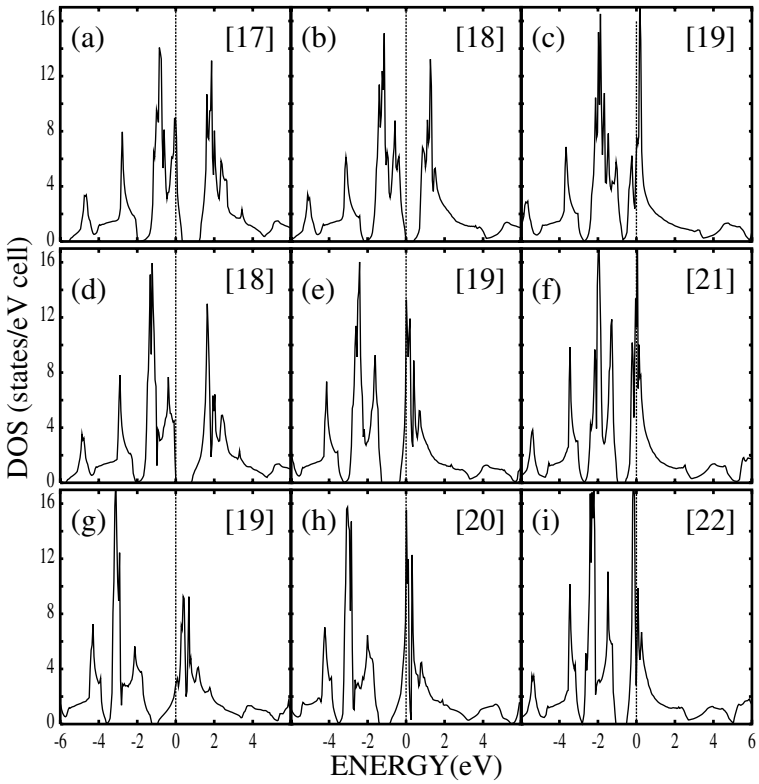

Figure 2. Total DOS in the paramagnetic state for (a) FeTiSb, (b) FeVSb, (c) FeMnSb, (d) CoTiSb, (e) CoVSb, (f) CoMnSb, (g) NiTiSb, (h) NiVSb, (i) NiMnSb. The number of valence electrons is indicated in the figure. All energies are w.r.t. the Fermi energy.

12 atoms of a similar kind at a distance of 7.79 au. In figure 3 (FeSb) the lowest three bands extending from -4 to -2 eV are the Sb p bands with the Sb s band lying far below the chosen scale of the figure. The Fe d bands are separated from the Sb p bands by a gap of approximate width 1.5 eV. Out of the available 13 valence electrons eight are accommodated in the Sb s–p complex and the rest are accommodated in the Fe d bands such that Fe e_g bands are completely full while Fe t_{2g} bands are one-sixth full. We have mapped the LDA band structure shown in figure 3 to an orthogonal tight-binding model where Fe d and Sb p orbitals are retained in the basis while Sb s and Fe s, p are downfolded. The range of this tight-binding model Hamiltonian is restricted to next nearest neighbour interaction (7.79 au) to provide reasonable agreement with the LDA bands [26]. The relative position of the Fe d levels with respect to the Sb p levels estimated from the on-site energy difference ($\varepsilon_d - \varepsilon_p$) is found to be 0.9 and 0.6 eV for Fe t_{2g} and Fe e_g respectively, resulting in a crystal field splitting ($\varepsilon_{e_g} - \varepsilon_{t_{2g}}$) to be -0.3 eV. In FeSb the four Sb atoms are tetrahedrally arranged for Fe and such an arrangement do not favour coaxial bonding, resulting in Sb-p–Fe-t_{2g} hybridization more favourable than the Sb-p–Fe-e_g hybridization. This strong covalent hybridization pushes the Fe t_{2g} bands to the top of the d bands while the Sb p bands are pushed below. This can be seen in figure 3 (FeSb), where the distribution of Sb p character outside the Sb p bands and vice versa from the Fe t_{2g} mixed into the Sb p bands indicates a strong covalent component in the bonding. Further, the less interacting Fe e_g bands where the interaction is mediated by weak pdπ hopping are narrow and lie almost dispersionless (flat) in most of the Brillouin zone. The dispersion of the

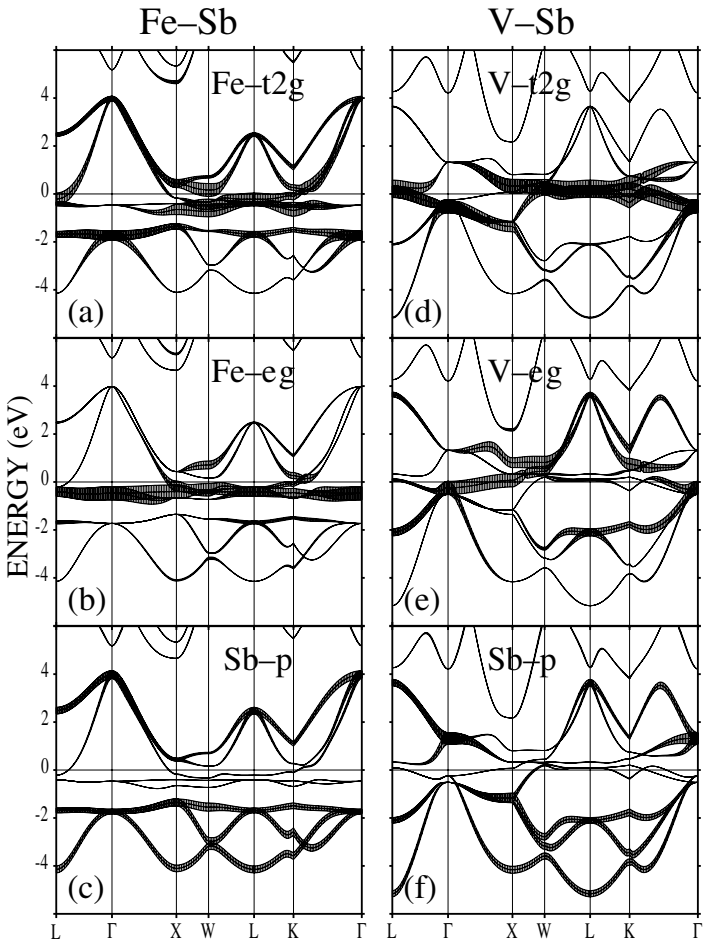

Figure 3. Orbital projected band structures of model binaries FeSb and VSb, decorated with Fe,V d e_g, t_{2g} and Sb p characters. All energies are w.r.t. the Fermi energy.

Fe t_{2g} bands is due mainly to hopping via Sb p orbitals, with negligible next nearest neighbour d–d hopping.

We consider next the binary VSb in the NaCl structure as displayed in figure 1(b). The nearest neighbour coordination for V (Sb) is six Sb (V) at a distance 5.51 au, while the next nearest neighbour coordination is 12 atoms of a similar kind like FeSb. From figure 3 (VSb) we find the lowest three broad bands extending from -5 to -1 eV are of Sb p character. Among the 10 valence electrons eight are accommodated in the Sb s–p bands and the remaining two electrons occupy the V d bands. The notable difference from FeSb is that the occupied Sb p bands are not separated from the V d bands by a gap, and both the V e_g as well as t_{2g} bands have appreciable dispersion. A tight-binding analysis for VSb yields values of V–Sb hoppings very similar to Fe–Sb hoppings; however, the relative position of the V d levels with respect to the Sb p levels is found to be 1.16 and 1.71 eV for V t_{2g} and V e_g respectively. The resulting crystal field splitting is 0.55 eV with the t_{2g} states lower in energy than the e_g states, as expected. The Sb atoms in the NaCl coordination with V favour strong pdσ interaction between Sb-p–V-e_g orbitals while the V t_{2g} orbitals only weakly hybridize with the Sb p orbitals. This can be seen

in figure 3 where the V t_{2g} bands remain unhybridized along W–L–K. Further, in the NaCl structure there is non-negligible V d–d as well as Sb p–p second nearest neighbour hopping which adds to the dispersion and to the band width of the V d as well as the Sb p bands. The above analysis suggests that the p–d gap in the FeSb binary is a precursor to the pseudo p–d gap seen in the ternary compounds in figure 2. Further, if now a hybridization is switched on between Fe and V, as expected in the FeVSb ternary, the d levels repel each other, resulting in a pair of bonding and antibonding bands separated by a gap. As mentioned earlier, if the number of valence electrons is such that the bonding complex is occupied we have a semiconductor.

With this background we shall now analyse the chemical bonding in the ternary compound FeVSb. In figure 4 we display the orbital projected band structures (fat bands) of FeVSb. The nearest neighbour coordination of Fe is 4 Sb and 4 V atoms. From figure 4, we can see, analogous to the binaries, that the lowest three bands are Sb p bands separated by a pseudo gap from five predominantly Fe d bands which in turn are separated from relatively broad V d bands by an indirect gap. A tight-binding analysis [26] retaining Fe d, V d and Sb p in the basis and restricting the range of interaction to 7.79 au, i.e. to the second nearest neighbour for Fe and the third nearest neighbour for V and Sb, provides reasonable agreement with the LDA bands shown in figure 4 as well as access to the various hoppings and the on-site energies. The relative positions of the Fe d and V d levels with respect to the Sb p levels are summarized as follows: Fe t_{2g} and e_g levels are at 0.71 and 0.66 eV respectively with negligible crystal field splitting while the V t_{2g} and e_g levels are at 1.44 and 2.15 eV respectively with appreciable crystal field splitting of about 0.71 eV. These relative positions of the Fe and V d levels are consistent with the relative positions of V and Fe in the periodic table, where V is three columns to the left of Fe. Since the Fe atoms are arranged tetrahedrally to V, so Fe-t_{2g}–V-t_{2g} interactions are more favourable. This can be observed from the fat bands where we see that along the high-symmetry direction W–L–K, the V t_{2g} band, which remains non-interacting and lies flat on the Fermi surface in the model binary substructure VSb, now strongly hybridizes with the Fe t_{2g} bands. As a result the higher-lying V t_{2g} bands are pushed above the Fermi level and open a way to form the gap at the Fermi level along W–L–K (see figure 4). At Γ, however, the top of the valence band is predominantly of V t_{2g} character and is below the Fermi level. The Fe e_g bands, which are weakly interacting with the V d bands along W–L–K, form a hole pocket at L (figure 4). In the model binary compound VSb, the bands along L–Γ–X that crossed the Fermi level between Γ–X have predominantly V e_g character now hybridize with the Fe e_g. This hybridization is strongest at Γ and weakest at X. Thus the band gets pushed above the Fermi level forming an electron pocket at X. Hence, we get an indirect band gap along X–L for the compound FeVSb. This is also true for other Fe-based half-Heusler alloys.

We shall now substantiate our argument by analysing the COHP plots which provide an energy-resolved visualization of the chemical bonding. As the name signifies, in COHP the density of states is weighted by the Hamiltonian matrix elements. The on-site COHP corresponds to the atomic contribution and the off-site COHP represents the covalent contribution to the bands. In figure 5 we display the site-projected DOS, as well as the off-site COHP, and the energy-integrated COHP (ICOHP) per bond for the nearest neighbour Fe–V, Fe–Sb and V–Sb interactions. The bonding contribution for which the system undergoes a lowering in energy is indicated by negative COHP and the antibonding contribution that raises the energy is represented by positive COHP. Thus it gives a quantitative measure of bonding. From the COHP plot in figure 5 we gather that the most dominant nearest neighbour interaction is between Fe and V. A comparison with the partial DOS reveals that the bonding and the antibonding states below and above the Fermi level are due to the nearest neighbour Fe–V interaction and this is the key interaction to open up a gap close to the Fermi level in these compounds. The occupied Sb states below the p–d gap are a result of Fe–Sb and V–Sb

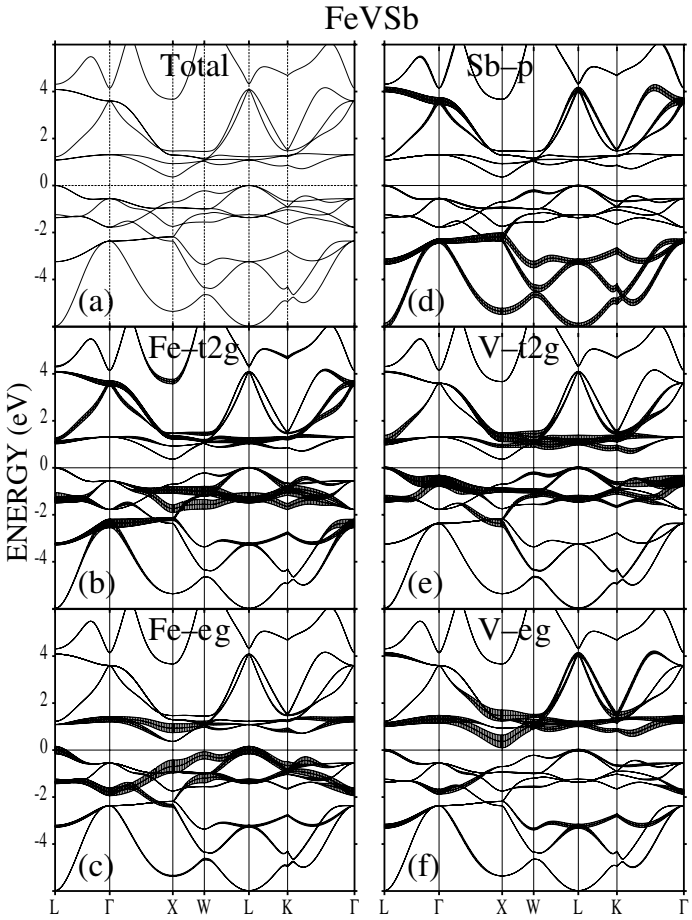

Figure 4. Band structure (a) and orbital projected band structure for FeVSb decorated with (b) Fe t_{2g}, (c) Fe e_g, (d) Sb p, (e) V t_{2g}, (f) V e_g. All energies are w.r.t. the Fermi energy.

bonding interactions with a relatively dominant contribution from the Fe–Sb interactions. The presence of Sb, which provides a channel to accommodate some TM d electrons in addition to its own sp electrons, is therefore crucial for the stability of these systems. This can be seen from the integrated COHP at the Fermi level for Fe–Sb (-1.8 eV) and V–Sb (-1.3 eV) interactions which adds to the minimization of the one-electron bond energy at the Fermi level.

We now compare our results for FeMSb with Co- and Ni-based compounds. We have considered two representative compounds, CoTiSb and NiTiSn, with 18 valence electrons and lattice constants slightly more than FeVSb (see table 2). In figure 6 we display the band dispersions for both these compounds along the same direction as for the Fe compound. Both compounds display a gap at the Fermi level. However, the crucial difference from the Fe compound is that the indirect band gap for the NiTiSn is now along ΓX instead of LX as seen for the Fe compounds. To understand this difference we have mapped the LDA band dispersion for CoTiSb and NiTiSn to an orthogonal tight-binding model as we have done for FeVSb. The analysis of the tight-binding parameters shows that the most notable difference among these compounds is the relative position of the TM d orbitals while the hoppings vary by only few per cent among the various compounds. We find

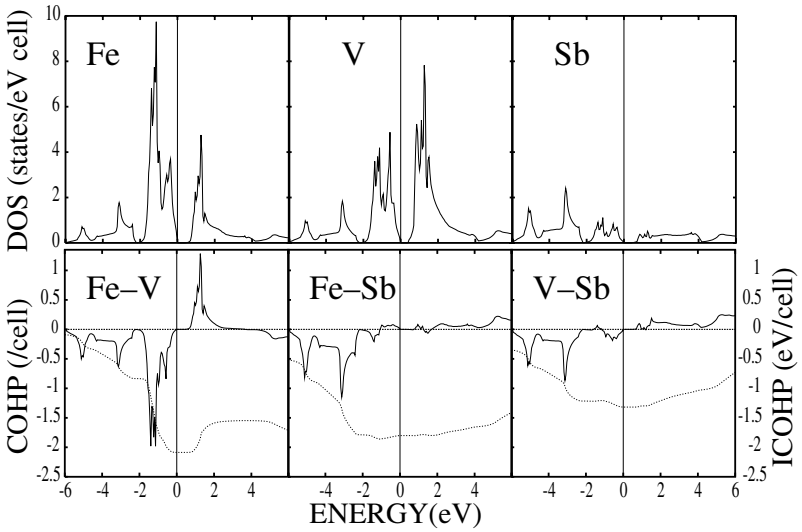

Figure 5. Site projected DOS (full curve), off-site COHPs (full curve) and integrated COHPs (ICOHP) (dotted curve) per bond for the nearest neighbour Fe–V, V–Sb and Fe–Sb. All energies are measured w.r.t. the Fermi energy.

ε(Ti d) $-$ ε(Ni d) (2.3, 3.4 eV) $>$ ε(Ti d) $-$ ε(Co d) (1.6, 2.7 eV) $>$ ε(V d)$-\varepsilon$(Fe d) (0.7, 1.5 eV), where in the parentheses we have indicated the values for the on-site energy difference between t_{2g} and e_g levels respectively. This trend in the difference of the on-site energies directly follows from the relative positions of the elements in the periodic table and has a profound effect on the band structure as it results in the Fe–V hybridization $>$ Co–Ti hybridization $>$ Ni–Ti hybridization. We find from the orbital character of the bands that at the X-point for both the Ni and the Co compounds the conduction band minimum at X is predominantly Ti t_{2g} (d_{xz}) in character, with the Ti e_g band above it. This is not the case for the FeMSb compounds, where M e_g constituted the conduction band minimum at X. However, the valence band maximum at Γ is predominantly Ti t_{2g} but now very much closer to the Fermi level for the Co and Ni compounds. These observations of close-lying (less separated) t_{2g} bands are consistent with the fact that the (Co, Ni)-d–M-d interaction is weaker in comparison to the Fe compound. This is also borne out in the COHP plot shown in figure 7. Analogous to the FeVSb we find the d–d interaction is crucial for opening up of the gap. Although the d–d COHPs are similar in shape to the Fe compound they differ in strength (e.g. ICOHP at the Fermi level for Fe–V, Co–Ti and Ni–Ti is -2.09 eV, -1.84 eV and -1.51 eV respectively) indicating that the covalent hybridization with M is strongest for Fe and weakest for Ni. Further, X(Fe, Co, Ni)–Z(Sb, Sn) and M–Z interaction is predominantly bonding, providing stability to the structure. In conclusion, the gap close to the Fermi level in the paramagnetic phase, which is crucial for many of the properties of the half-Heusler phases, arises from the covalent hybridization between the d states of the higher-valent TM X with the d states of the lower-valent TM M. A similar finding has been reported in [16, 27].

Finally, in figure 8 we present the total DOS and the COHP plots per bond for the nearest neighbour Fe–V, Fe–Sb and V–Sb interactions in the β (SbVFe) and the γ (VFeSb) phase for FeVSb in order to understand the reason for the stability of the α phase as revealed in our total energy calculations. We note both in the β and the γ phase the system is metallic. Further, in either configuration V–Sb is in the diamond substructure which enhances the V–Sb interaction, as can be seen from the COHP plot in figure 8. This contributes to the V bandwidth. In addition

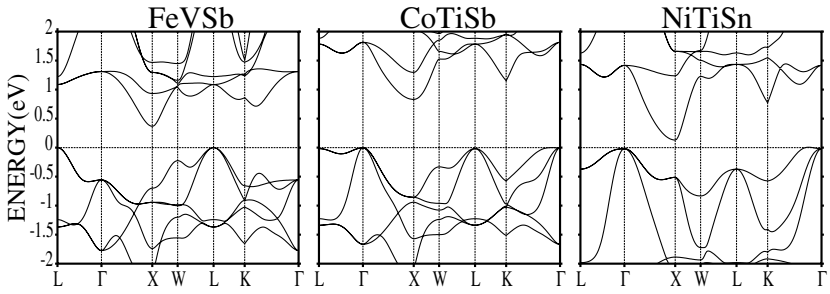

Figure 6. Band structure in a narrow scale for the 18-electron compounds FeVSb, CoTiSb and NiTiSn. All energies are w.r.t. the Fermi energy.

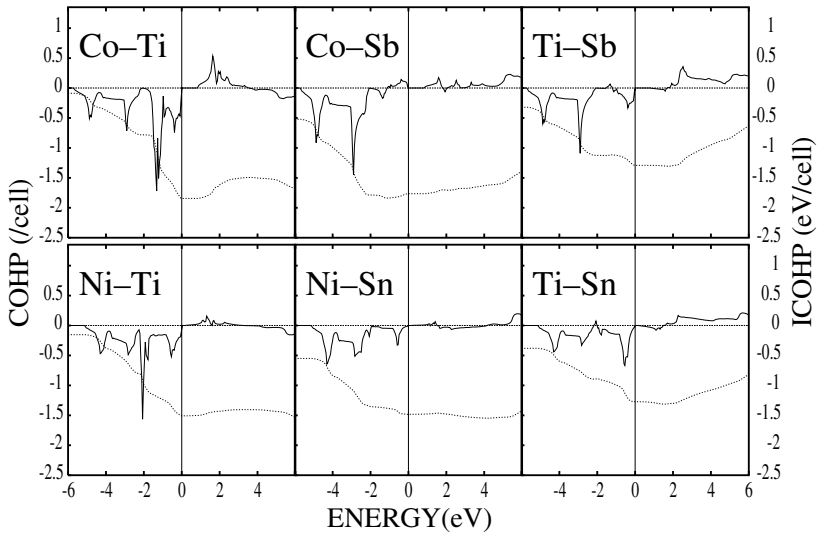

Figure 7. COHPs (full curve) and ICOHPs (dotted curves) per bond for the nearest neighbour CoTiSb and NiTiSb. All energies are w.r.t. the Fermi energy.

the Fe–V interaction is now too weak to produce a gap at the Fermi level, making both these systems energetically less favourable, consistent with our total energy calculations.

4. Spin-polarized calculations

The magnetic properties of half-Heusler compounds range from paramagnetic metals, ferromagnetic metals to half-metallic ferromagnets and ferrimagnets. In this section, we shall analyse the electronic structure of half-Heusler phases to elucidate their novel magnetic properties. Our analysis is based on spin-polarized DOS and COHP studies.

Before we analyse our spin-polarized calculations, let us summarize briefly the salient features of the paramagnetic calculations that are conducive to magnetism. The characteristic feature of all half-Heusler compounds is a d–d gap close to the Fermi level. All the states below this gap are occupied for the 18-VEC compounds. However, if the number of valence electrons is more than 18, then the Fermi level is at the antibonding complex and if the density of states is high at the Fermi level then the paramagnetic state becomes unstable and stability can be achieved by developing magnetic order. This is due to the fact that upon spin

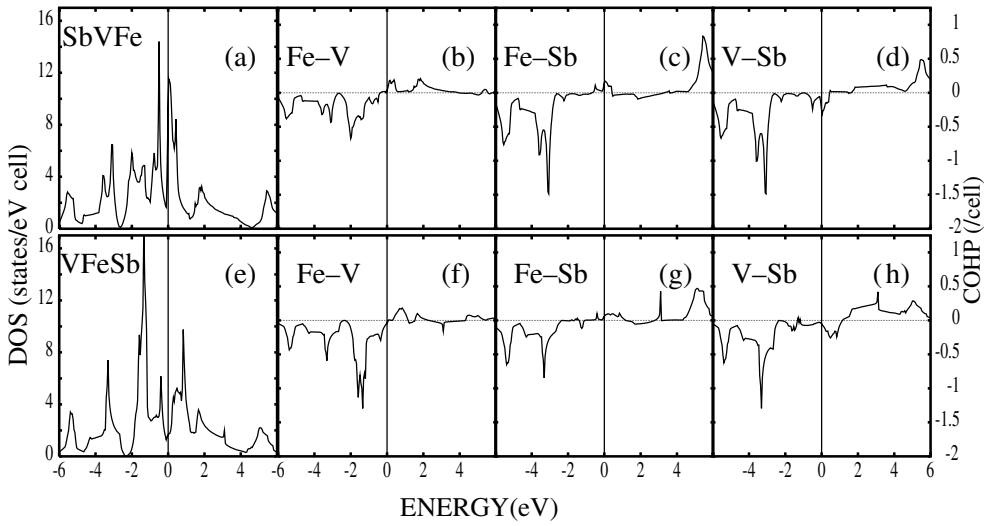

Figure 8. Total DOS and COHPs per bond for the nearest neighbour β and γ phase for FeVSb. All energies are w.r.t. the Fermi energy.

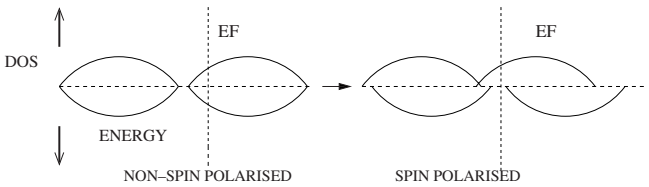

Figure 9. Schematic diagram within rigid band model relevant for the half-Heusler phases.

polarization, the electrons arrange themselves so that the spontaneous magnetization makes the spin-up and spin-down electrons different, and lowers the overall bonding energy to make the system stable. Within the Stoner model for ferromagnetism, the magnetism is a result of competition between two energies: (i) increase in the kinetic energy as the electrons are forced to occupy the higher bands, due to the rearrangement of the occupation of the majority and the minority spin electrons, and (ii) overall reduction of the Coulomb repulsion. However, as argued in [15], if the paramagnetic DOS supports a gap as in the half-Heusler alloys then there exists an interesting possibility shown schematically in figure 9. Now in the process of spin polarization the depletion of the minority band may be such that only the minority bonding states below the d–d gap are occupied leading to complete spin polarization and we have a half-metallic ferromagnet. As a result, the magnetic moment also increases with the increase in the number of valence electrons.

Figure 10 displays the total DOS for several Fe-, Co- and Ni-based half-Heusler compounds and table 4 summarizes the magnetic moments. We discover the following trends from the DOS plot for the compounds with more than 18 valence electrons considered here: (i) the d–d gap persists at the minority spin channel for all the compounds and (ii) for Fe, Co and Ni, if M is Mn or Cr, then the system is half-metallic, in good agreement with the previous calculations reported by others [1, 12, 16]. However, for compounds (VEC >18) with early 3d elements, like Ti and V, we find CoVSb is half-metallic, while NiTiSb is non-magnetic and NiVSb is magnetic (they do not exhibit half-metallic behaviour). The compounds

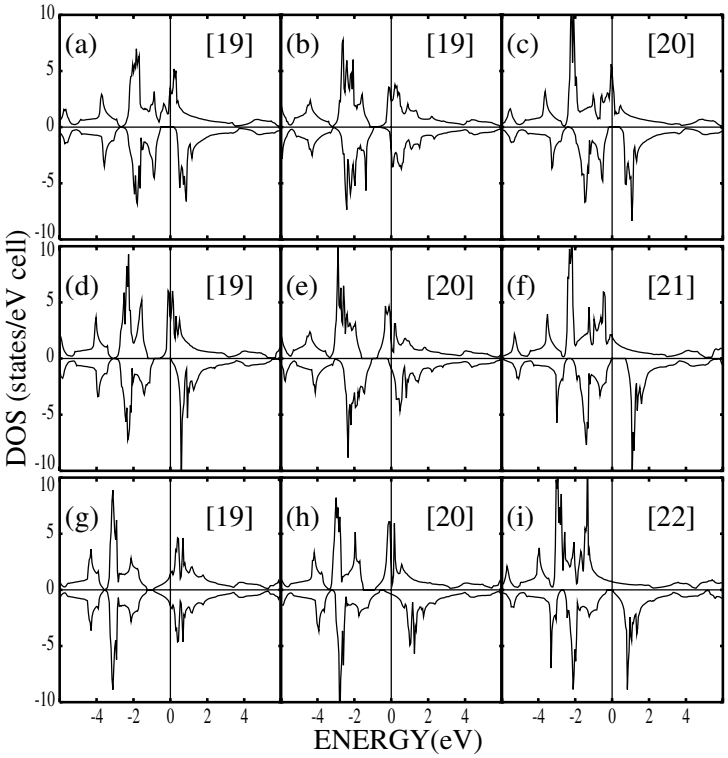

Figure 10. Spin-polarized total DOS for (a) FeCrSb, (b) FeMoSb, (c) FeMnSb, (d) CoVSb, (e) CoMoSb, (f) CoMnSb, (g) NiTiSb, (h) NiVSb, (i) NiMnSb. All energies are w.r.t. Fermi level.

with M as a 4d element, like Mo, are also not half-metallic but are magnetic. In the last column of table 4 we have calculated the extent of half-metallicity (HM) at E_{F} defined as $\mathrm{HM} = \frac{D_{\uparrow}(E_{\mathrm{F}})-D_{\downarrow}(E_{\mathrm{F}})}{D_{\uparrow}(E_{\mathrm{F}})+D_{\downarrow}(E_{\mathrm{F}})} \times 100\%$ where $D(E_{\mathrm{F}})$ is the DOS at the Fermi level. We note from the values of HM in the last column of table 4 that Mn and Cr are important for stabilizing half-metallic ferromagnetism in these systems. The reason for this may be attributed to the large exchange splitting in Mn and Cr which can be seen from figure 11, where we have plotted the X and M partial density of states and off-site COHP per bond for the nearest neighbour pairwise X–M interactions in both the spin channels for the compounds FeMnSb, FeCrSb, CoMnSb, CoMoSb, NiMnSb and NiVSb. We gather from figure 11 that (i) the exchange splitting is much larger for Cr and Mn in comparison with V and Mo and (ii) the Mn and Cr majority spin states are almost completely occupied, while the minority spin states are nearly empty. This localized exclusion of the spin-down states from the Mn and Cr sites manifests as a localized region of magnetization [28], proving crucial for the half-metallic character. In the half-metallic state nine electrons are accommodated in the minority spin bands, and the excess of 18 electrons are all accommodated in the antibonding majority bands thereby contributing to the magnetic moment. This can be seen in table 4 for the compounds FeCrSb, FeMnSb, CoMnSb and NiMnSb, where the magnetic moment increases by integral amounts with increase in the number of valence electrons.

We shall now consider the spin-resolved COHP plots presented in figure 11. We note in the minority spin channel that the X(Fe, Co, Ni)–M interaction is strongest for Fe and weakest for Ni. This trend is similar to the paramagnetic calculations discussed in section 3. This implies

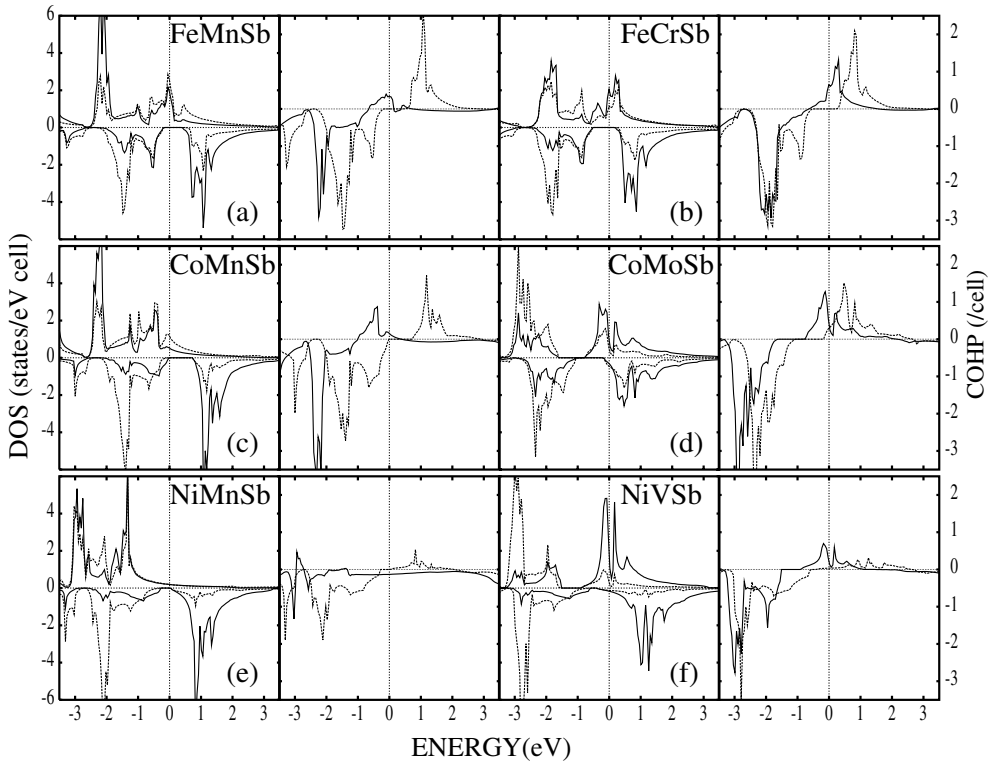

Figure 11. Spin-polarized partial DOS (left) and X(Fe, Co, Ni)–M(Mn,Cr, V, Co) COHP (right) for (a) FeMnSb, (b) FeCrSb, (c) CoMnSb, (d) CoMoSb, (e) NiMnSb, (f) NiVSb. Mn/Cr/Mo/V-d DOS and spin-up COHPs are shown by solid curves and Fe/Co/Ni-d DOS and spin-down COHPs are shown by dotted curves. All energies are w.r.t. Fermi energy.

that hybridization between Fe–Mn is stronger than Co–Mn, which in turn is stronger than Ni–Mn. As a consequence the minority valence band has a larger Mn admixture for Fe that for Co and Ni, while the constitution of the majority bands is barely changed. This results in the reduction of the magnetic moment at the Mn site for FeMnSb in comparison with CoMnSb and NiMnSb as can be seen from table 4. Further, Fe and Co moments are now negative, making these systems half-metallic ferrimagnets while NiMnSb is a half-metallic ferromagnet.

In the majority spin channel we learn from the COHP plots that the X–M interaction at the Fermi level is weakly antibonding for FeCrSb, FeMnSb and CoMnSb but bonding for NiMnSb. A comparison of the DOS (E_F) for FeCrSb, FeMnSb, CoMnSb and NiMnSb in the majority spin channel also shows that it is quite appreciable for Fe and Co compounds and it is minimum for NiMnSb. This indicates that NiMnSb is the most stable compound while FeCrSb, FeMnSb and CoMnSb are possibly unstable or difficult to prepare and if prepared may be subject to electronic or structural instabilities. In fact experimentally CoMnSb is reported to be a ferromagnetic metal [29] with a large magnetic moment. It has been suggested that either CoMnSb crystallizes in a more complex structure [30] or there is appreciable disorder in the sample leading to a disorder phase of the type X_2MZ. Spin-polarized KKR-CPA calculations [31] on the hypothetical system $(Co_{0.5}E_{0.5})_2MnSb$, where E is a vacancy, agree quite well with experiment.

Further, we gather from table 4 that for XMSb (X = Fe, Co, Ni, M = Cr, Mn, V, Ti) the magnetic moment at the X site is much smaller in comparison to the M site. The 3d band width

Table 4. Magnetic moments (in μ_B) of several Fe-, Co- and Ni-based half-Heusler compounds (HM, extent of half-metallicity).

Compounds (VEC)	Mag. mom. Fe/Co/Ni (μ_B)	Mag. mom. M (μ_B)	Mag. mom. Sb/Sn (μ_B)	Mag. mom. total (μ_B)	HM (%)
FeCrSb(19)	−0.552	1.585	−0.033	1.000	100
FeMoSb(19)	0.248	0.363	0.016	0.632	6
FeMnSb(20)	−0.394	2.455	−0.055	2.000	100
CoVSb(19)	−0.073	1.065	−0.021	0.988	100
CoNbSb(19)	0.000	0.000	0.000	0.000	0
CoMoSb(20)	0.650	1.111	0.037	1.820	23
CoMnSb(21)	−0.075	3.176	−0.112	3.000	100
NiTiSb(19)	0.000	0.000	0.000	0.000	0
NiVSb(20)	0.118	1.714	−0.022	1.822	68
NiMnSb(22)	0.320	3.720	−0.059	4.000	100

of pure TMs decreases with increasing nuclear charge whereas the intraatomic correlations (or exchange) increase; however, for the half-Heusler phases, as we have pointed out, there is an appreciable hybridization of the X atom with the M and the Sb atom, which contributes to the bandwidth of the X atom and may therefore be much more effective in screening the intraatomic correlations. The presence of the gap in the paramagnetic state increases the kinetic energy cost for the rearrangement of the occupation of the minority and majority spin states of the X atom. It is interesting to note that in the β and the γ phase of FeMnSb, where the d–d gap does not exist and the hybridization of Fe with Mn and Sb is substantially reduced, FeMnSb does not exhibit half-metallic ferromagnetism and Fe also acquires a sizable magnetic moment. Hence the d–d gap, the hybridization of X with M and Sb which is maximized in the α phase together with the large exchange splitting at the M site are crucial ingredients to induce half-metallic properties in these systems.

5. Summary and conclusions

We have applied the FP-LMTO method as well as the TB-LMTO ASA method to investigate in detail the electronic structure, chemical bonding and magnetism of a series of half-Heusler compounds XMZ, where X = Fe, Co, Ni, M = Ti, V, Nb, Cr, Mo, Mn and Z = Sn, Sb. We have analysed in detail the physical origin of the gap in the paramagnetic as well as in the spin-polarized state in these compounds. The relative position of the atoms in the unit cell, which influences the gap, has also been studied. Our detailed analysis employing various indicators of chemical bonding suggests covalent hybridization of the higher-valent transition element X with the lower-valent transition element M is the key interaction responsible for the formation of the so-called d–d gap in these systems separating the bonding states from the antibonding states. The presence of the sp-valent element is crucial as it not only hybridizes with X and M but also provides a channel to accommodate extra d electrons responsible for the stability of these systems. The correspondingly larger hybridization of Sb with X accounts for the relative stability of the α phase where the higher-valent transition element X is at the octahedrally coordinated pocket in the NaCl substructure formed by MSb and is also responsible for the novel magnetic properties. The Sb s–p states and the bonding subbands can accommodate 18 electrons; as a consequence some of the systems with 18 valence electrons are semiconducting. Systems with more than 18 electrons are magnetically stable. We show that the X–M hydridization is strongest for Fe and weakest for Ni, which reflects itself in the nature of the indirect band gap in these systems.

We have also investigated in detail some of the systems with more than 18 valence electrons which exhibit novel magnetic properties, namely half-metallic ferro- and ferrimagnetism, ideal for spintronic applications. We show that the gap in the paramagnetic state, appreciable X–Sb and X–M hybridization and large exchange splitting of the M atoms are responsible for the half-metallic property of these systems. Based on this understanding it will be interesting to investigate the role of dilute magnetic impurities like Mn and Cr in semiconducting half-Heusler compounds. Our preliminary investigation [26] indicates that some of these systems are indeed half-metallic, and in a future communication we shall explore this scenario in more detail.

Acknowledgments

We thank G P Das and D D Sarma for useful discussions. BRKN thanks CSIR, India, for research fellowship (JRF). The research is funded by CSIR (grant no. 03(0931)/01/EMR-II).

References

[1] Webster P J and Ziebeck K R A 2001 *Alloys and Compounds of d-Elements with Main Group Elements* (*Landolt–Börnstein New Series* Group III, Vol. 19c Part 2) ed H P J Wijn (Berlin: Springer) pp 75–184
[2] de Groot R A, Mueller F M, van Engen P G and Buschow K H J 1983 *Phys. Rev. Lett.* **50** 2024
[3] Prinz G A 1995 *Phys. Today* **48** 54
Prinz G A 1999 *J. Magn. Magn. Mater.* **200** 57
Wolf S A, Awschalom D D, Buhrman R A, Daughton J M, von Molnar S, Roukes A Y, Chtchelkanova A Y and Treger D M 2001 *Science* **294** 1488
[4] Larson P, Mahanti S D, Sportouch S and Kanatzidis M G 1999 *Phys. Rev.* B **59** 15660
[5] Hohl H, Ramirez A P, Goldmann C, Ernst G, Wolfing B and Ernst B 1999 *J. Phys.: Condens. Matter* **11** 1697
[6] Uher C, Yang J, Hu S, Morelli D T and Meisner G P 1999 *Phys. Rev.* B **59** 8615
[7] Young D, Khalifah P, Cava R J and Ramirez A P 2000 *J. Appl. Phys.* **87** 317
[8] Xia Y, Ponnambalam V, Bhattacharya S, Pope A L, Poon S J and Tritt T M 2001 *J. Phys.: Condens. Matter* **13** 77
[9] Ogut S and Rabe K M 1995 *Phys. Rev.* B **51** 10443
[10] Larson P, Mahanty S D and Kanatzidis M G 2000 *Phys. Rev.* B **62** 12754
[11] Tobola J, Pierre J, Kaprzyk S, Skolozdra R V and Kouacou M A 1998 *J. Phys.: Condens. Matter* **10** 1013
[12] Tobola J and Pierre J 2000 *J. Alloys Compounds* **296** 243
[13] Tobola J, Jodin L, Peucheur P and Scherrer H 2001 *Phys. Rev.* B **64** 155103
[14] Ishida S, Masaki T, Fujji S and Asano S 1997 *Physica* B **237/238** 363
[15] Jung D, Koo H-J and Whangbo M-H 2000 *THEOCHEM* **527** 113
[16] Galankis I, Dederichs P H and Papanikolaou N 2002 *Phys. Rev.* B **66** 134428
[17] Savrasov S Y 1990 *Phys. Rev.* B **54** 16470
[18] Andersen O K and Jepsen O 1984 *Phys. Rev. Lett.* **53** 2571
Jepsen O and Andersen O K 2000 *The Stuttgart TB-LMTO-ASA Program, Version 47*
[19] Perdew J P, Burke K and Ernzerhof M 1996 *Phys. Rev. Lett.* **77** 3865
[20] Jepsen O and Andersen O K 1971 *Solid State Commun.* **9** 1763
Jepsen O and Andersen O K 1984 *Phys. Rev.* B **29** 5965
[21] Von Barth U 1972 *J. Phys. C: Solid State Phys.* **5** 1629
Hedin L 1971 *J. Phys. C: Solid State Phys.* **4** 2064
[22] Jepsen O and Andersen O K 1995 *Z. Phys.* B **97** 35
[23] Dronskowski R and Blochl P E 1993 *J. Phys. Chem.* **97** 8617
Boucher F, Jepsen O and Andersen O K, unpublished
[24] Evers C B H, Richter C G, Hartjes K and Jietschko W 1997 *J. Alloys Compounds* **295** 93
[25] de Groot R A and Buscho K H J 1986 *J. Magn. Magn. Mater.* **54–57** 1377
[26] Nanda B R K and Dasgupta I 2003 unpublished
[27] Nanda B R K, Deepa K and Dasgupta I 2001 *Proc. DAE Solid State Symp.* vol 44, p 313
[28] Kubler J, Williams A R and Sommers C B 1983 *Phys. Rev.* B **28** 1745
[29] Otto M J, Feil H, Van Woerden R A M, Wijngaard J, Van Der Valk P J, Van Bruggen C F and Hass C 1987 *J. Magn. Magn. Mater.* **70** 33
[30] Senateur J P, Rouault A, Fruchart R and Fruchart D 1972 *J. Solid State Chem.* **5** 229
[31] Kaczmarska K, Pierre J, Tobola J and Skolozdra R V 1999 *Phys. Rev.* B **60** 373